Thermoeconomic analysis and optimization of a novel geothermal based multi generation system for electricity generation, cooling, heating and hydrogen liquefaction

Ali Eyvazi[1*], Mehran Ameri[2] , Mohammad Shafiey Dehaj[3] and Hadi Ghaebi [4]

[1*] Phd student, Department of Mechanical Engineering, Faculty of Engineering, Vali-e-Asr University of Rafsanjan, Rafsanjan, Iran

[2] Professor, Department of Mechanical Engineering, Faculty of Engineering, Shahid bahonar University of Kerman, Kerman, Iran

[3] Associate Professor, Department of Mechanical Engineering, Faculty of Engineering, Vali-e-Asr University of Rafsanjan, Rafsanjan, Iran

[4] Professor, Department of Mechanical Engineering, Faculty of Engineering, University of Mohaghegh Ardabili, Ardabi, Iran

Abstract

This evaluation presents an integrated, renewable multi generation system powered by geothermal energy. The system incorporates a double-flash geothermal unit, two ejector cooling cycles, a proton exchange membrane electrolyzer, an absorption precooling cycle, and a Claude hydrogen liquefaction subsystem. The study investigates a geothermal-based multi generation system utilizing a double-flash cycle to generate power, provide cooling capacity, and produce liquefied hydrogen. The performance of the proposed system is assessed based on energy, exergy, and economic factors. A case study analyzed the system's behavior under specific conditions. Additionally, a sensitivity analysis was performed to understand how varying operating conditions impacted the system's performance. Finally, a two-objective genetic algorithm, combined with the TOPSIS decision-making method, was employed to optimize the proposed system. The results of the thermodynamic evaluation indicate that the energy efficiency of the proposed system is 16.2%, while the exergy efficiency is 54.1%. This system is anticipated to produce hydrogen at a rate of 0.4 kg per hour, with a measured output power of 105 kW. The analysis reveals that the work required for the hydrogen liquefaction cycle is 7.784 kW, and the total exergy destruction within the studied system amounts to 3437 kW. The economic analysis shows a total system cost of $37.60 per GJ, underscoring its strong financial viability. Additionally, the levelized cost of electricity generation is 24.58, and the levelized cost of hydrogen production is 23.92, further demonstrating the system's robust thermodynamic performance and economic feasibility.

Keywords: Claude cycle; Ejector; Heat recovery; Hydrogen; Genetic algorithm

1.Introduction

Global energy demand has surged dramatically, resulting in an increased reliance on fossil fuels for energy production. The combustion of these fuels emits greenhouse gases, which contribute to environmental pollution. As a result, renewable energy sources have gained considerable attention as a viable solution to the challenges posed by fossil fuel dependency [1]. These renewable energy sources, derived from natural and readily available resources, help reduce our reliance on petroleum and mitigate environmental pollution. As energy demands continue to rise, the global development and adoption of renewable resources become essential. Poorly designed buildings significantly contribute to energy consumption and negatively impact both human health and the environment. Therefore, prioritizing renewable resources is crucial for meeting the energy needs of buildings [2]. Although fossil fuels have played a crucial role in industrialization and national development, their contribution to establishing a stable global economy is limited. While they offer short-term benefits to consumers, the long-term consequences of fossil fuel use are detrimental to humanity, impacting lifestyles through changes in home heating and lighting. The increased global expansion, industrialization, and demands of developing nations have led to a significant rise in fossil fuel consumption. This surge has, in turn, released substantial pollutants such as nitrogen oxides, carbon dioxide, and carbon monoxide, which contribute to environmental issues like acid rain, ozone depletion, and rising global temperatures. Nearly half of the carbon dioxide emitted globally results from the combustion of fossil fuels for electricity generation. The potential of renewable energy is constrained by limited resources and challenges in energy storage, which can lead to decreased stability in the power supply [3]. Additionally, renewable electricity production faces higher initial costs due to the need for backup systems and ongoing maintenance expenses, in contrast to traditional energy sources. These costs are somewhat mitigated by environmental benefits and reduced expenditures on fossil fuels. However, the undervaluation of renewable energy output and the low prices of fossil fuels pose significant barriers to the increased adoption of renewable energy. To enhance the prominence of renewable fuels, several strategies can be implemented. These include eliminating subsidies for fossil fuels, dismantling monopolies in electricity production, promoting private sector participation, providing tax incentives, and ensuring the procurement of newly developed energy sources. Renewable energy is particularly vital in developing countries, where it plays a critical role in economic policy and in meeting the energy needs of factories and industrial regions. Even amid the current energy crisis, renewable energy continues to be a significant contributor to the overall energy supply. The efforts of developing countries to reduce their dependence on non-renewable fuel exports for economic stability highlight the ongoing significance of fossil fuels. In contrast, geothermal energy harnesses heat from beneath the Earth's surface, utilizing water or steam as the transport medium [4]. Geothermal power plants generally demonstrate lower efficiency compared to fossil fuel and hydroelectric plants, primarily due to steam temperatures that typically remain below 250°C and the presence of non-condensable gases. Their efficiency is further influenced by the power generation cycle used and the temperature of the geothermal reservoir. Notably, hydrothermal plants that employ dual cycles exhibit particularly low

efficiency, ranging from 2.8% to 5.5%. Steam geothermal power plants are geographically limited because they rely on specific geological conditions. However, recent technological advancements have enabled the commercialization of small-scale dual-cycle power plants. Geothermal power plants eliminate the need for fuel combustion, leading to lower infrastructure costs and significantly reduced environmental pollution. While the efficiency of geothermal power plants is approximately 15% due to the low pressure and temperature of the steam, fossil fuel power plants typically achieve efficiencies closer to 35%. Locating geothermal plants near steam production sources minimizes heat loss in pipelines. A 100 MW geothermal plant utilizes 80 tons of steam per hour from wells drilled into a shared reservoir. The rate of steam condensation from the turbine exceeds the evaporation rate of the cooling tower, allowing the condensed water to be recycled as makeup water for the cooling tower, thereby reducing reliance on external water sources. Both the condenser and the cooling tower release non-condensable gases into the atmosphere. Within the hydrothermal system, water flows into a separator, where it generates steam that is subsequently used to drive the turbine. Excess water discharged from the cooling tower is pumped back into the well. Although constructing the power plant and geothermal wells simultaneously requires a significant initial investment, the cost of geothermal power is expected to decrease as the reliability of steam availability improves. Geothermal power plants can adjust their output to meet energy demands by controlling the number of active production wells. This energy source provides consistent power that is unaffected by weather conditions and is available at all times [5]. Geothermal energy systems offer high electrical efficiency and the capability to generate clean power [6]. Additionally, geothermal systems are highly efficient in electricity generation, making them an attractive option for both heating and cooling applications [7]. Geothermal power plants play a significant role in reducing environmental pollution and greenhouse gas emissions [8,9]. Kianfard et al. [10] demonstrated a geothermal energy-driven multi-production system for generating hydrogen and fresh water, which is projected to recover its investment in 5.6 years. Akrami et al. [11] investigated a geothermal-based system designed for the simultaneous production of power, hydrogen, and cooling. Their results indicated that the system exhibits an energy efficiency of 34.98% and an exergy efficiency of 49.17%. Yuksel et al. [12] investigated a cogeneration system designed for the simultaneous production of power, hydrogen, and cooling. They found that increasing the hot source temperature from 130°C to 200°C improved hydrogen generation from 0.03 to 0.07. Ghaebi et al. [13] reported that a geothermal-based cogeneration system achieved an energy efficiency of 94.98% and an exergy efficiency of 47.89%. Yilmaz et al. [14] investigated a multi-generation system powered by geothermal energy. This system incorporated a proton exchange membrane (PEM) water electrolysis unit for hydrogen production. They discovered that the geothermal heat preheated the water for electrolysis to 80°C, enabling the system to generate 0.034 kg/s of hydrogen. Similarly, Hai et al. [15] examined a geothermal-powered multi-generation system designed for electricity generation, cooling, heating, and hydrogen production. They reported an energy efficiency of 24.4%, an exergy efficiency of 32.1%, and a hydrogen production rate of 0.9662 kg/s. Sangsaraki et al. [16] investigated a novel cogeneration system

that utilizes geothermal energy to produce both electricity and hydrogen. Their research demonstrated that, with a geothermal source, this system can achieve an exergetic efficiency of 25.27%, generate a net power output of 4.03 MW, and produce liquid hydrogen at a rate of 59.92 kg/h. Kaskan et al. [17] examined a hybrid system that incorporates a dual-flash geothermal unit, reporting an energy efficiency of 10.6% and an exergetic efficiency of 59.3%. Abdul Ali Pouradel et al. [18] found that a multi-generational system utilizing a double-flash cycle produced 8.6 MW of net power and 2.308 kg/h of hydrogen. Rostamzadeh et al. [19] investigated a geothermal multi-generation system utilizing a two-stage organic Rankine cycle, achieving an energy efficiency of 39.02% and an exergetic efficiency of 25.09%. Pan et al. [20] evaluated the use of zeotropic mixtures in a geothermal cogeneration system, concluding that a pentane/isohexane mixture attained an exergetic efficiency of 58.33% and generated 1.9 MW of net power. Zhang et al. [21] conducted a study on a geothermal multi-generation system designed to simultaneously produce electricity, cooling, fresh water, and hydrogen. This system employed an Organic Rankine Cycle unit, utilizing zeotropic mixtures as the working fluid. Specifically, the R12-R114 mixture achieved a net power output of 856.06 kW, a hydrogen generation rate of 0.743 kg/h, and a cooling capacity of 2410.54 kW. The system's energy efficiency was measured at 17.84%, while its exergy efficiency was recorded at 32.24%. Yilmaz et al. [22] investigated a multi-generation system powered by geothermal energy that produced electricity, cooling, heating, and freshwater. Their study demonstrated that the system could generate 298 kW of electricity, 1,169 kW of cooling, 2.77 kg/s of freshwater, and 0.000392 kg/s of hydrogen. The energy efficiency and exergy efficiency of the system were found to be 42.48% and 38.26%, respectively. Heydaranjad et al. [23] enhanced a geothermal power plant by integrating biomass, aiming to produce both clean energy and potable water. A crucial aspect of this enhancement was the combustion of urban solid waste, which significantly improved the system's performance. The exhaust gases generated from this waste combustion powered a multifunctional desalination subsystem. The research demonstrated that the integrated system achieved energy and exergy efficiencies of 13.9% and 19.4%, respectively. An economic analysis revealed that the total cost of the system was $285.30 per hour. Additionally, an environmental assessment indicated that utilizing urban solid waste instead of coal reduced carbon dioxide emissions by 8,092 tons and nitrogen oxide emissions by 36 tons. Kahraman et al. [24] conducted a thermodynamic study on a geothermal power plant integrated with air conditioning. This research examined the impact of varying ambient air temperatures on the plant's total production costs, energy efficiency, and exergy. The results indicated that while power generation could reach 6.8 MW as the ambient temperature increased from 5 to 35 °C, the system's cost rate also increased. Yilmaz et al. [25] designed integrated plant systems that analyze the thermodynamic and environmental impacts of producing clean and sustainable electricity, heating, green hydrogen, and distilled water using geothermal energy. Their proposed system integrates a double-flashing geothermal cycle, a reheat CO2 Rankine cycle, a multi-effect distillation desalination unit, and a proton exchange membrane electrolysis system. The results indicated that the system is capable of producing green hydrogen at a rate of 0.004595 kg/s, with

an energy efficiency of 18.40% and an exergy efficiency of 17.71%. Yilmaz et al. [26] investigated a novel geothermal energy system designed as a multigeneration plant for the production of clean and sustainable products. Their proposed system features a re-compression supercritical Brayton power plant, an ejector cooling unit, a humidifier-dehumidifier desalination unit, a proton-exchange membrane process, and a hot water preparation unit. The designed system results in annual CO_2 emissions of 117 tonnes. Additionally, the energetic and exergetic efficiencies of the presented microgrid plant have been determined to be 14.09% and 23.35%, respectively. Dan et al. [27] evaluated an integrated, renewable geothermal-powered multigeneration system that includes a double-flash unit, a modified dual-pressure organic Rankine cycle, a proton exchange membrane electrolyzer, and a Claude hydrogen liquefaction subsystem. They demonstrated a total cooling load generation of 2.27 MW, a net output power of 10.48 MW, and a liquefied hydrogen production rate of 37.83 kg/h. The system also exhibited an exergetic efficiency of 55.89%, with an exergy destruction rate of 9.39 MW. Despite numerous evaluations of geothermal multigeneration systems for power generation, cooling, and hydrogen production, there are significant opportunities to optimize the utilization of geothermal energy across a wider range of applications. The implementation of high-efficiency thermodynamic combined cycles to harness power from existing heat sources is a crucial element of sustainable energy strategies. Previous research has primarily concentrated on single-well combined cycle configurations, resulting in a significant gap in our understanding of systems that integrate multiple wells with varying temperature and pressure profiles. Geothermal well water is initially expanded instantaneously through distinct processes and then directed to separator tanks for utilization throughout the cycle. A dual ejector cycle is incorporated into the main system to enhance the power and exergy derived from the well's outlet fluid. The net power output and efficiency of the combined cycle are influenced by the outlet pressures of the expansion valve. Utilizing an ejector to minimize heat loss in the expansion valve enhances both the system's output power and overall efficiency. The useful work produced by the turbine constitutes the net power of the combined cycle. The net power output of the cycle is directly proportional to the useful work performed by the turbine. This investigation contributes to the existing literature by proposing a completely emission-free cogeneration system that harnesses geothermal energy for the simultaneous generation of power and hydrogen. This study explores the use of an absorption heat transformer to enhance low-temperature heat derived from geothermal sources. The resulting higher-temperature heat will subsequently drive a generation cycle that ultimately supplies energy for a proton exchange membrane hydrogen production process.

This study explores an innovative multigeneration system that utilizes a dual geothermal source, incorporating a double-flash geothermal unit, two ejector cooling cycles, a proton exchange membrane electrolyzer, an absorption precooling cycle, and a Claude hydrogen liquefaction subsystem. The performance of the proposed system is evaluated through a multidimensional analysis that considers energy, exergy, and economic factors. The energy analysis in this case study examines net power output, liquid hydrogen production rate, system cooling load, and energy efficiency. These parameters are crucial for assessing the energy performance of the

proposed configuration. Additionally, an exergy analysis is conducted to evaluate the quality of the system's performance, with the goal of optimizing the work output of the cycle. This analysis also effectively identifies inefficiencies and potential improvements within the system. Furthermore, an economic analysis assesses the system's profitability. Optimizing the studied system necessitates a comprehensive understanding of thermoeconomics, which combines thermodynamic and economic factors. By applying economic principles to technical design, we can identify and implement operating conditions that aim to minimize total production costs. The ejector refrigeration cycle employs two evaporators that function at different cooling temperatures: one below zero degrees Celsius and one above. Each evaporator is specifically designed to handle distinct cooling loads, which were not addressed in previous studies. The novelty in this research lies in the recovery of waste heat from the turbine through a heat exchanger, which is simultaneously utilized to provide cooling capacity for both the lower ejector refrigeration cycle and the absorption precooling cycle. In addition, the implementation of two ejector cooling cycles minimizes exergy destruction in the power generation unit of the proposed system, representing another innovative aspect of this study. This research introduces a novel method for generating liquid hydrogen that incorporates the recovery of excess heat for cooling purposes. The hydrogen production in the electrolyzer is powered by geothermal energy. Furthermore, a heat exchanger recovers waste heat from the geothermal source, resulting in the generation of additional electricity. The single-effect absorption cooling unit reduces energy consumption in liquid hydrogen production by pre-cooling the hydrogen stream with heat recovered from the heat exchanger. The system's thermodynamic efficiency is further enhanced by immersing this pre-cooled hydrogen gas in a liquid nitrogen bath.

2. System description

Figure 1 illustrates the proposed multigeneration system designed for the production of electricity, cooling, hot water, and hydrogen. The system consists of a double-flash geothermal unit, two ejector cooling cycles, a proton exchange membrane electrolyzer, an absorption precooling cycle, and a Claude hydrogen liquefaction subsystem. In the initial stage, high-pressure and high-temperature geothermal water is extracted from the production well. Subsequently, an expansion valve reduces the pressure of this fluid to match the pressure within the flash chamber. Inside the flash chamber, the geothermal fluid is separated into brine and steam. This steam is directed to the turbine, where it generates power. The exhaust from the turbine is routed to Ejector 1 as its primary flow, supplying a cooling charge at -5°C, which is suitable for freezing. This primary flow within the ejector subsequently draws in the secondary flow into the mixing chamber. After undergoing several internal processes, the mixed flow is released at the designated back pressure. This discharged stream is then cooled in Condenser 1 and subsequently divided into two distinct flows. The first pathway involves expanding the stream with an expansion device and then cooling it to its freezing temperature using Evaporator

1, which generates a cooling load for the freezing process. The second pathway directs the remaining flow to the re-injection well. The cooled saturated liquid is routed to the second ejector to create a cooling charge at 5°C. Within the ejector, the ejected stream undergoes a process before being condensed into a liquid in Condenser 2. The liquid output is divided into two distinct streams. After expansion through a dedicated device, one stream undergoes evaporation in Evaporator 2. This process generates a cooling effect suitable for non-freezing applications, while the remaining portion of the flow is directed to the re-injection well. The heat exchanger captures excess heat, which is then used to pre-cool the absorption chiller in a single-effect process. This pre-cooling reduces the energy required for liquid hydrogen production. The pre-cooled water subsequently flows into the electrolyzer, where hydrogen gas is generated. The hydrogen gas is then directed into the compressor within the liquefaction cycle. After compression, the high-pressure hydrogen gas is separated into two distinct streams. One of these streams passes through Heat Exchanger 1, where it is cooled by the cold vapor returning from the separator. Heat Exchanger 2 utilizes nitrogen vapor to cool the remaining hydrogen. The hydrogen then flows to the pre-cooler, where it is cooled by liquid nitrogen. Finally, it passes through another heat exchanger, where it is cooled by steam from the separator. The separator divides the mixture into liquid and vapor phases, and the resulting liquid hydrogen is stored in the source.

Fig.1. Schematic view of the proposed system

3. Methodology

A comprehensive thermodynamic and economic model of the multi-generation system was developed in this study. The modeling process utilized Engineering Equation Solver (EES) software, which provides functions for calculating thermodynamic properties. The thermodynamic equations are solved simultaneously under the assumption of a steady state. The economic analysis section involves updating all pricing and inflation parameters to provide a robust justification for the plan. Subsequently, a parameter test will be conducted to assess the impact of variations in the system's primary functions. The optimization process will focus on two objective functions: exergy efficiency and cost, with the aim of achieving optimal overall system performance.

4. Thermodynamic modeling

The thermodynamic analysis of the system under consideration includes the following assumptions [28,29]:

• Conditions remain stable throughout the process.

• The steam turbine and compressor operate at isentropic efficiency.

• It is assumed that enthalpy remains constant before and after the expansion valve.

• Outputs from the evaporator and condenser are assumed to be in a saturated state.

The proposed multigeneration system is modeled using mass, energy, and exergy balance equations. Necessary data for the simulation are presented in Table 1.

Table. 1. Thermodynamic operating parameters of the system

parameter	value
Ambient temperature (℃)	25
ambient pressure (kPa)	101.3
Geothermal fluid inlet temperature (℃)	170
geothermal fluid inlet pressure (kPa)	900
Geothermal fluid input mass flow rate	10
Flash chamber pressure (kPa)	500
Isentropic efficiency of steam turbine (%)	70
Steam turbine outlet pressure (kPa)	100
Condenser 1 temperature (℃)	25
Condenser 2 temperature (℃)	25
Evaporator 1 temperature (℃)	-5
Evaporator 2 temperature (℃)	5
Compressor compression ratio	20
Compressor isentropic efficiency (%)	80
Ejector nozzle efficiency (%)	85
Ejector mixer efficiency (%)	9
Ejector diffuser efficiency (%)	85

The mathematical relationships for modeling the ejector, which were developed in prior research and are summarized in Table 2 [30], were applied in this study. Using these equations, an iterative technique was implemented to calculate the mass entrainment ratio of the ejector.

Table. 2. Mathematical relations used for the ejector [30]

system components	Exergy destruction equation
Ejector mass bubble ratio	$\mu = \dfrac{m_{sf}}{m_{pf}}$
Ejector pressure increase ratio	$\pi_{eje} = \dfrac{p_{ex}}{p_{sf}}$
Isentropic efficiency of moving nozzle	$\eta_{sf} = \dfrac{h_{pf} - h_{noz}}{h_{pf} - h_{noz,is}}$
Energy balance between the nozzle section and the primary fluid	$= \dfrac{1}{2} v_{noz}^2 h_{pf} - h_{noz}$
Conservation of momentum in the mixing section	$V_{mf} = \dfrac{v_{noz}}{1 + \mu}$
Energy balance for the ejector	$h_{out} = \dfrac{h_{pf} + h_{sf}\,\mu}{1 + \mu}$
Mixing efficiency	$\eta_{mix} = \dfrac{v_{mf,s}^2}{v_{mf}^2}$
Energy balance equation between the mixing and outlet sections	$h_{out} - h_{mf} = \dfrac{1}{2} v_{mf,is}^2$
Diffuser efficiency	$= \dfrac{h_{out,is} - h_{mf}}{h_{out} - h_{mf}}\eta_{dif}$

The mass and energy balance for the proposed system is calculated using the assumptions detailed in the following equations:

$$\sum m_i = \sum m_e \tag{1}$$

$$Q - W = \sum m_e h_e - \sum m_i h_i \tag{2}$$

The following equation provides the method for calculating the specific flow of exergy:

$$ex_{ph} = (h - h_0) - T_0(s - s_0) \tag{3}$$

The following equation is used to determine the operation of a PEM electrolyzer [31]:

$$W_{PEM} = 0.25 \times W_{Total} \tag{4}$$

The amount of hydrogen produced is calculated using the following equation:

$$M_{H2_{out}} = a_{H2} \times W_{PEM}{}^{bH2} + c_{H2} \tag{5}$$

$$= 0.0036 \times M_{H2_{out}} \tag{6} \quad N_{H2_{out}}$$

The coefficients a, b, and c are 3.382, 0.97, and 5.928, respectively. These values are used in the following relationships to calculate the energy efficiency and exergy of the system being studied.

$$\eta_{energy} = \frac{W_{total} + Q_{evaporator} + m_{35}h_{35}}{m_1 h_1 + m_{19}h_{19}} \tag{7}$$

$$= \frac{W_{total} + Q_{evaporator}((\frac{T_0}{T_{evaporator}}) - 1) + m_{35}e_{35}}{m_1 e_1 + m_{19}e_{19}} \tag{8} \ \eta_{exergy}$$

Thermodynamic inefficiencies in thermal systems arise from exergy destruction and loss. Exergy analysis identifies the system components and processes that exhibit the greatest thermodynamic inefficiencies. Generally, reducing inefficiencies in a component is advantageous unless it leads to increased overall capital or fuel costs in other areas. Energy conservation efforts should focus on components with the highest potential for improvement. The complete set of exergy destruction balance equations for the components of the proposed multigeneration system is presented in Table 3.

Table. 3. Exergy destruction relations of different components of the system

component	exergy destruction equation
Absorption cooling cycle absorber	$-\dot{E}_{26} - Q_{ABS}(1 - \frac{T_0}{T_{ABS}})\dot{E}_{25} + \dot{E}_{31}$
Absorption cooling cycle generator	$-\dot{E}_{29} + \dot{E}_{20} - \dot{E}_{21} + Q_{gen}(1 - \frac{T_0}{T_{gen}})\dot{E}_{28} - \dot{E}_{22}$
Absorption cooling cycle condenser	$-\dot{E}_{23} - Q_{Cond}(1 - \frac{T_0}{T_{cond}})\dot{E}_{22}$
Absorption cooling cycle evaporator	$-\dot{E}_{25} + Q_{evap}(1 - \frac{T_0}{T_{evap}})\dot{E}_{24}$
Absorption cooling cycle vapor heat exchanger	$-\dot{E}_{28} - \dot{E}_{30}\dot{E}_{27} + \dot{E}_{29}$
Rankine cycle condenser1	$-\dot{E}_8 - Q_{Cond1}(1 - \frac{T_0}{T_{cond}})\dot{E}_7$
Rankine cycle evaporator1	$-\dot{E}_6 + Q_{Evap1}(1 - \frac{T_0}{T_{evap}})\dot{E}_{10}$
Rankine cycle evaporator2	$-\dot{E}_{13} + Q_{Evap2}(1 - \frac{T_0}{T_{evap}})\dot{E}_{17}$
Rankine cycle turbine	$-\dot{E}_5 - W_{turb}\dot{E}_3$
Rankine cycle condenser2	$-\dot{E}_{15} - Q_{Cond2}(1 - \frac{T_0}{T_{cond}})\dot{E}_{14}$
PEM Electrolyzer	$-\dot{E}_{35} + W_{Electrolizer}\dot{E}_{33} - \dot{E}_{34}$
heat exchanger	$-\dot{E}_{12} - \dot{E}_{20}\dot{E}_4 + \dot{E}_{21}$
PEM heater	$-\dot{E}_{33} - \dot{E}_{19}\dot{E}_{18} + \dot{E}_{32}$

Claude cycle compressor	$-W_{Comp\,act} W_{Comp\,rev}$
Claude cycle heat exchanger 1	$-\dot{E}_{39}\dot{E}_{38} + \dot{E}_{47} - \dot{E}_{48}$
Claude cycle heat exchanger 2	$-\dot{E}_{50}\dot{E}_{39} + \dot{E}_{49} - \dot{E}_{40}$
Claude cycle heat exchanger 3	$-\dot{E}_{47}\dot{E}_{46} + \dot{E}_{40} - \dot{E}_{41}$
Claude cycle heat exchanger 4	$-\dot{E}_{42}\dot{E}_{51} + \dot{E}_{41} - \dot{E}_{52}$
Claude cycle heat exchanger 5	$-\dot{E}_{46}\dot{E}_{42} + \dot{E}_{45} - \dot{E}_{43}$
Claude cycle super heater	$\dot{E}_{44} - \dot{E}_{45} - \dot{E}_{53}$
Valve 1	$\dot{E}_{1} - \dot{E}_{2}$
Valve 2	$\dot{E}_{9} - \dot{E}_{10}$
Valve 3	$\dot{E}_{16} - \dot{E}_{17}$
Flash chamber	$\dot{E}_{2} - \dot{E}_{3} - \dot{E}_{4}$
Ejector1	$\dot{E}_{5} + \dot{E}_{6} - \dot{E}_{7}$
Ejector2	$\dot{E}_{12} + \dot{E}_{13} - \dot{E}_{14}$

5. Economic analysis

Thermoeconomic analysis, commonly employed in energy systems, simultaneously evaluates both economic and thermodynamic performance. This analysis assesses costs to identify inefficiencies and determine the economic viability of system components. Such evaluations help identify areas for improvement, optimize designs, and ensure efficient resource utilization [32]. While increasing investment can enhance the efficiency of energy conversion systems, it is crucial to find the right balance between cost and productivity gains [30]. The previous review analyzed both energy and exergy values at specific points within the system. Additionally, developing separate cost equations is essential to ensure that expenses are allocated appropriately among the various components of the system. The following relationship offers a method for calculating the investment rate and capital maintenance requirements [34]:

$$Z_k = CRF \times \frac{\varphi_r}{(N \times 3600)} \times PEC_k \tag{9}$$

The variables φ, N, and PEC represent the maintenance factor, the operating time over one year, and the investment cost of the component, respectively. Additionally, the CRF parameter denotes the capital recovery factor, the value of which is derived from the following equation.

$$CRF = \frac{i(1+i)^n}{(1+i)^n - 1} \tag{10}$$

The thermoeconomic assessment of thermodynamic systems utilizes various functions [35]. The following relationship illustrates the correlation between the levelized cost of energy (LCOE) and the levelized cost of hydrogen (LCOH) for the system examined in this study [36]:

$$\text{LCOE} = \frac{AOC}{(W_{total} + Q_{cooling} + Q_{heating}) \times \tau} \tag{11}$$

$$\text{LCOH} = \frac{AOC}{((LHV_{H_2} \dot{N}_{H_2} \dot{m}_{H_2}) + Q_{cooling} + Q_{heating}) \times \tau} \tag{12}$$

The variable τ represents the system's annual operating hours, typically estimated at 8,000 hours per year. The annual operating cost (AOC) is subsequently calculated using the following method [37]:

$$\text{AOC} = (\text{TOC} \times \varphi \times \text{CRF}) \tag{13}$$

The total system cost per hour is calculated by dividing the annual expenses by the estimated 7446 working hours in a year [38].

$$Z_{Toatal} = (\text{TOC} \times \varphi \times \text{CRF})/t \tag{14}$$

Economic analysis helps business owners understand the current economic environment and its impact on their company's potential for success. Table 4 presents a method for calculating the purchase cost of each system component illustrated in Fig. 1. Considering the expected operational lifespan of each component, the cost rate measured in \$/GJ serves as a valuable metric for analysis [39].

Table. 4. cost functions of different components of the system [39]

component	cost function
Absorption cooling cycle generator	$z = 17500 \times \left(\frac{A_{Gen}}{100}\right)^{0.6}$
Absorption cooling cycle condenser	$z = 8000 \times \left(\frac{A_{Cond}}{100}\right)^{0.6}$
Absorption cooling cycle absorber	$z = 16000 \times \left(\frac{A_{Absorb}}{100}\right)^{0.6}$
Absorption cooling cycle evaporator	$z = 16000 \times \left(\frac{A_{Evap}}{100}\right)^{0.6}$
Absorption cooling cycle steam heat exchanger	$z = 12000 \times \left(\frac{A_{SHE}}{100}\right)^{0.6}$
Organic Rankine Cycle Condenser	$z = 516.62 \times (A_{Cond})^{0.6}$

Turbine	$z = 4750 \times (W_{Turb})^{0.75}$
Evaporator	$z = 4122 \times (A_{Evap})^{0.6}$
heat exchanger	$z = 4122 \times (A_{heat\ exchanger})^{0.6}$
Claude cycle compressor	$z = 7900 \times (W_{Comp})^{0.62}$
Claude cycle heat exchanger	$z = 8500 + 409 \times (A_{heat\ exchanger})^{0.8}$
PEM electrolyzer cycle	$Z = 1000 \times (W_{elec})$

6. Two-objective optimization with genetic algorithm

Genetic algorithms are optimization and search techniques inspired by the principles of natural selection and genetics. They enhance a population of solutions by applying selection criteria to minimize a cost function. This study conducted a two-objective optimization using genetic methods to identify the most efficient operational mode of the proposed system. The use of a genetic algorithm facilitates the exploration of optimal conditions for all design variables, ultimately leading to the identification of the best system parameters. Minimizing the total cost rate and maximizing exergy efficiency are fundamental optimization objectives. Consequently, a key area of research in energy systems involves optimizing the performance of multiple generation systems to achieve these goals. Several parameters influence the system's performance. Among these, steam turbine outlet pressure, flash chamber pressure, and turbine isentropic efficiency are identified as critical decision variables. Parameters for a genetic algorithm were configured, specifically utilizing a mutation method. Mutation involves random alterations in individuals, with each minor change referred to as a mutation step. These steps are applied to variables based on a low probability known as the mutation rate. The likelihood of a variable undergoing mutation decreases as its dimensionality increases. Increasing the number of dimensions reduces the likelihood of a mutation occurring. However, the mutation rate remains unaffected by population size. Selecting the appropriate jump step size poses a significant challenge. The ideal step size is dependent on the specific problem and varies throughout the optimization process. While using small jump steps often leads to progress, employing larger jump steps can potentially yield better outcomes more efficiently. A suitable jump operator should be designed to incorporate either a small jump step with a high application rate or a large jump step with a low application rate. Determining the optimal operating point for system performance necessitates a criterion to assess potential candidates. In this study, the Technique for Order of Preference by Similarity to Ideal Solution (TOPSIS) was chosen as the decision-making criterion. The derivation of a relationship between cost rate and efficiency offers a framework for understanding and predicting the impact of each objective on the other. In the context of multi-objective optimization and Pareto analysis, the entire Pareto curve represents a

collection of optimal solutions. Consequently, the final choice of solution is influenced by the decision maker's policies, which can result in different designs selecting various points based on their specific requirements. For two-objective optimization problems, the point on the Pareto front that minimizes the distance to the ideal point is typically chosen as the final optimal solution. Deviation from the ideal point along the Pareto front results in a monotonic increase in cost in one direction and a significant decrease in efficiency in the other. Multi-objective optimization addresses the presence of multiple objective functions, while two-objective optimization involves two inherently conflicting objectives; improving one objective necessarily degrades the other. The Pareto diagram clearly displays the optimal point identified using the TOPSIS decision criterion. Furthermore, the diagram effectively illustrates the interaction between the two objective functions by plotting them against one another.

7. Validation

This research presents a novel approach to organizing a simultaneous production system. To validate the proposed system, an evaluation was conducted using the findings of Arora et al. [40] as a benchmark, and the results were further compared with those detailed in Table 5. Both this study and the aforementioned research will be analyzed by modeling the described processes. The models will be based on initial conditions and assumptions, including an ambient temperature of 25 °C and an ambient pressure of 101 kPa. The results will then be compared. The changes in pressure and heat due to passage through the system components are negligible. Under equilibrium conditions, the solutions exiting the absorber and generator are assumed to be saturated with respect to their individual temperatures and concentrations. The refrigerant leaving the condenser is considered saturated, as is the vapor exiting the evaporator, both at their respective saturation temperatures. The refrigerant vapor leaving the generator is in a superheated state and is at the generator's temperature. This analysis utilizes actual conditions, including non-equilibrium states at the inlets of the generator and absorber, as well as the states at the outlets of the solution pump and solution heat exchanger. It is assumed that the temperatures of the heat source and generator are equal. The refrigerant has a mass flow rate of 1 kg/s, and the generator operates at a temperature of 87.8°C. The evaporator temperature is recorded at 7.2°C, while both the condenser and absorber operate at 37.8°C. The results of the comparison reveal a slight difference, indicating a high level of accuracy in the validation.

Table .5. Validation of the proposed system with the evaluation of Arora et al. [40]

Parameter	obtained results	Reference results
absorbent heat (kW)	2943	2945.26
condenser heat (kW)	2506	2505.91
evaporator heat (kW)	2355	2355.4
coefficient of performance	0.79	0.7609
absorptive exergy destruction (kW)	70.16	70.478
condenser exergy destruction (kW)	6.606	6.066
evaporator exergy destruction (kW)	86.28	86.275

8. Results

Thermodynamic modeling of the proposed system was conducted using EES software. The energy and exergy analysis, detailed in Table 6, revealed an energy efficiency of 16.2% and an exergy efficiency of 54.1%, indicating the system's high performance.

Table. 6. Results of thermodynamic evaluation

parameter	value
energy efficiency (%)	16.2
exergy efficiency (%)	54.1
LCOE(cent/kWh)	24.58
LCOH($/kg)	23.92
Hydrogen production (kg/hr)	0.4
Absorption cooling cycle work (kW)	5.644
Liquefaction cycle work (kW)	7.784
Electrolyzer work (kW)	39.98
Total system work (kW)	105

The exergy destruction of various components within the system is evaluated by simulating the thermodynamic properties at different points using EES software. According to the findings presented in Table 7, the total exergy destruction for the proposed system is 3437 kW. The PEM electrolyzer experiences the highest exergy destruction, while Evaporator 1 exhibits the least exergy loss among all system components.

Table. 7. Exergy destruction results of different components of the system

parameter	value
PEM electrolyzer (kW)	363.5
evaporator of the absorption cooling cycle(kW)	86.29
turbine (kW)	298.6
condenser of absorption cooling cycle(kW)	6.62
Condenser 1 (kW)	5.56
Condenser 2 (kW)	14.79
absorption cooling cycle generator(kW)	49.96
expansion valve of the absorption cooling cycle(kW)	6.934
vapor heat exchanger absorption cooling cycle(kW)	6.33
heat exchanger (kW)	819.5
Claude cycle Compressor(kW)	45.22
Claude cycle heat exchanger 1(kW)	66.58
Claude cycle heat exchanger 2(kW)	14.07
Claude cycle heat exchanger 3(kW)	79.67
Claude cycle heat exchanger 4(kW)	6.328
Claude cycle heat exchanger 5(kW)	117.4
evaporator1(kW)	0.31
evaporator2(kW)	3.88
valve1(kW)	883.7
valve2(kW)	1.09
valve3(kW)	4.98
super heater(kW)	103.1
flash chamber(kW)	27.39
ejector1(kW)	156.4
ejector2(kW)	161.5
total system (kW)	3437

The proposed system is analyzed from an economic perspective, and revised cost functions are established for its various components to ensure high economic efficiency across different applications. Table 8 presents the results of the economic analysis, including the costs associated with the different components of the system. Among the components evaluated, the electrolyzer represents the largest portion of the overall system cost, while Ejector 1 is the least expensive component.

Table. 8. Cost functions results of different components of the system

parameter	value
PEM electrolyzer ($/GJ)	5038574
evaporator of the absorption cooling cycle($/GJ)	36134
turbine ($/GJ)	179178
condenser of absorption cooling cycle($/GJ)	11291
Condenser 1 ($/GJ)	29508
Condenser 2 ($/GJ)	53177
absorption cooling cycle generator($/GJ)	17484
vapor heat exchanger absorption cooling cycle($/GJ)	9322
heat exchanger ($/GJ)	68682
claude cycle Compressor($/GJ)	28194
claude cycle heat exchanger 1($/GJ)	8834
claude cycle heat exchanger 2($/GJ)	8549
claude cycle heat exchanger 3($/GJ)	8520
claude cycle heat exchanger 4($/GJ)	8516
claude cycle heat exchanger 5($/GJ)	8609
evaporator1($/GJ)	27794
evaporator2($/GJ)	79441
absorber of the absorption cooling cycle($/GJ)	31992
ejector1($/GJ)	6475
ejector2($/GJ)	195315

8.1 Parametric analysis

Parametric analysis is a reliable method for evaluating a system's performance under various operating conditions, providing a comprehensive understanding of its behavior. Specifically, this analysis examines how key design parameters—such as the isentropic efficiencies of the turbine and compressor, turbine outlet pressure, and compressor compression ratio—affect the performance of the system under investigation.

8.1.1 Effect of turbine isentropic efficiency changes on system performance

Figure 2 examines the effects of varying turbine efficiency on several key system parameters: power output, hydrogen production, cost rate, and both exergy and energy efficiency. The results indicate that increasing turbine efficiency from 0.6 to 0.8 leads to a higher total net power output from the system and an increase in liquid hydrogen production. The rise in power and hydrogen production is directly associated with improved turbine efficiency. Since the turbine serves as the primary source of electricity, and the electrolyzer relies on this electricity to produce hydrogen, a more efficient turbine generates more electricity, which in turn enhances the electrolyzer's performance and results in increased hydrogen output. Enhancing turbine efficiency has improved the exergy efficiency of the system, but it has also led to an increase in the system's cost rate. The observed rise in exergy rate is directly related to the positive correlation between exergy efficiency and system output power; greater work output from the system results in a higher exergy rate. Several factors contribute to the increase in cost rates. The expansion of system capacity and the need for larger equipment directly elevate system costs. Furthermore, higher overall production costs, escalating energy expenses, and the financial implications of system downtime also play a significant role. The production capacity was not cost-effective, as each subsystem contributed to the overall expenses, resulting in an increased total system cost. Exergy represents the maximum potential work that a system can produce. In this context, exergy specifically refers to the useful work extracted by the turbine. Variations in total work directly affect exergy efficiency, either increasing or decreasing it accordingly.
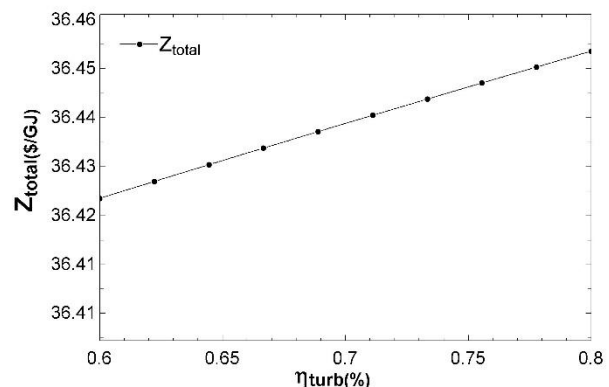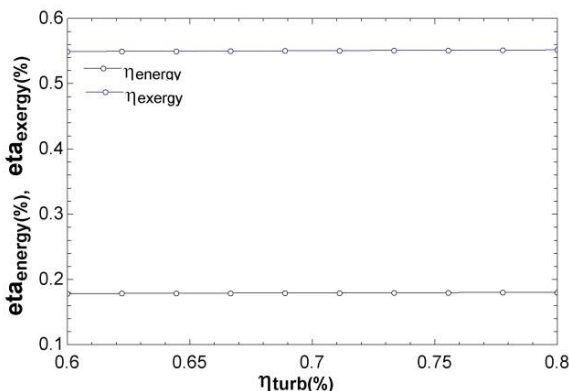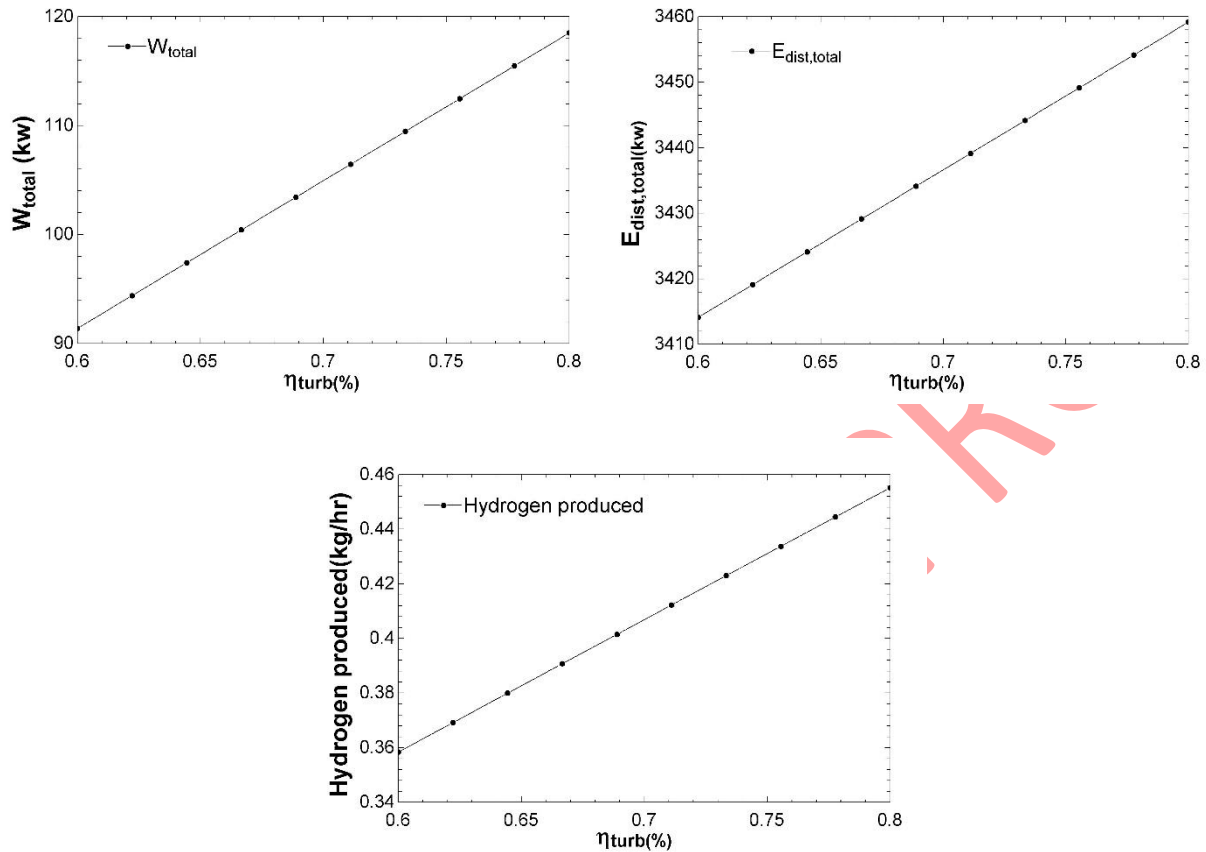
Fig.2. Effect of turbine isentropic efficiency changes on system performance

8.1.2 Effect of turbine output pressure changes on system performance

The relationship between turbine output pressure and system performance is illustrated in Figure 3. Increasing the pressure from 40 kPa to 60 kPa, as shown in Figure 9, resulted in a 15% decrease in the system's electricity production capacity and a 20% reduction in hydrogen production capacity. These observations suggest a correlation between saturation temperature and ejector pressure; specifically, the saturation temperature increases as the ejector pressure rises. This effect elevates the temperature of the geothermal fluid at the ejector, which subsequently reduces the heat transfer from the geothermal fluid to the ejector cycle. The diminished heat transfer leads to a decrease in cycle mass flow rates. The elevated temperature of the incoming geothermal fluid to the absorption cooling generator enhances the cooling capacity of the absorption cooling cycle. Figure 3 illustrates the relationship between turbine output pressure and system performance. Higher output pressures lead to lower cycle mass flow rates and reduced system capacities, ultimately resulting in decreased exergy destruction and increased

exergy efficiency. Although the increase in turbine output pressure lowers total costs, it also significantly reduces electricity and hydrogen production capacity, making this reduction the primary outcome.
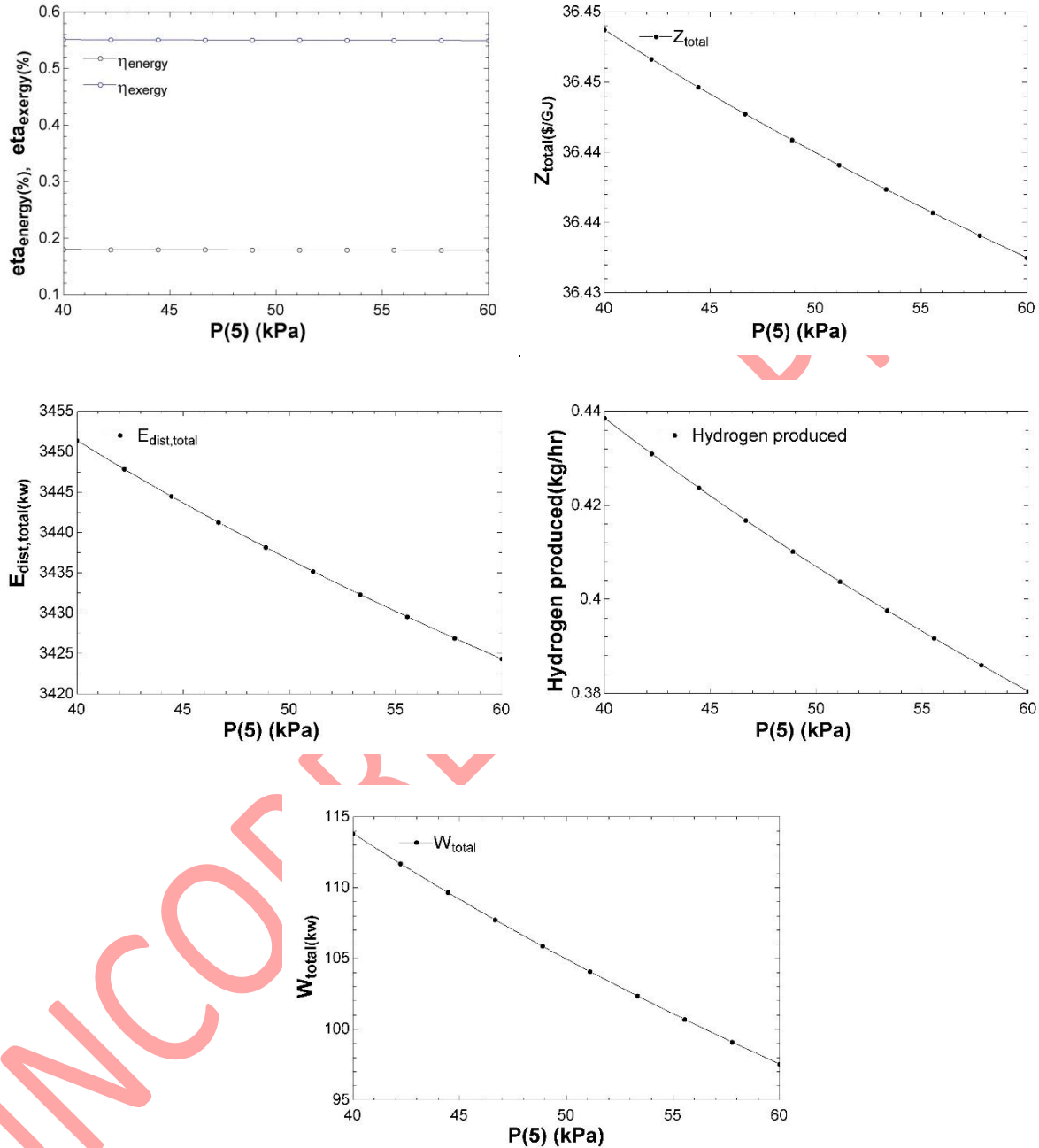
Fig.3. Effect of turbine output pressure changes on system performance

8.1.3 Effect of compressor compression ratio changes on system performance

<mark>Figure 4 illustrates the operational behavior of each component of the Combined Cooling, Heating, and Power (CCHP) system as a function of the compressor pressure ratio. As the pressure ratio increases, power production initially rises, reaches a peak, and then declines. The work required by the air compressor is lower at lower pressure ratios compared to higher ones. Additionally, the rate of increase in compressor work is slower at lower pressure ratios. This interaction leads to net power production reaching a maximum before decreasing as the pressure ratio continues to rise. Moreover, exergy destruction significantly decreases with an increasing pressure ratio. The primary reason is that a higher pressure ratio diminishes the difference in exergy between the compressed air and the compressor discharge. As the compression ratio increases, cold production rises, heat production decreases, and net power initially increases at lower compression ratios before declining at higher ratios. With an increase in the compression ratio, both energy efficiency and exergy efficiency improve, while total exergy destruction within the system decreases. Although energy efficiency increases, the overall system cost also rises with an increase in the compression ratio.</mark>
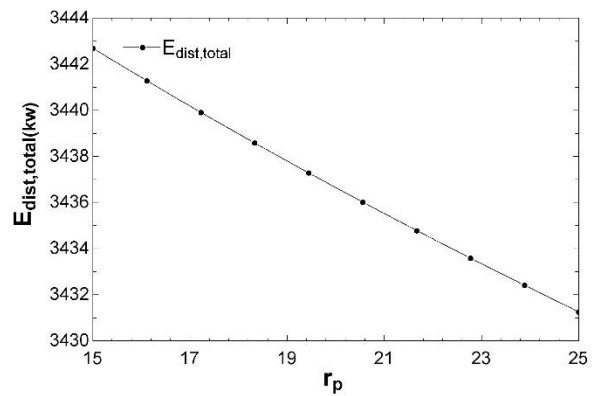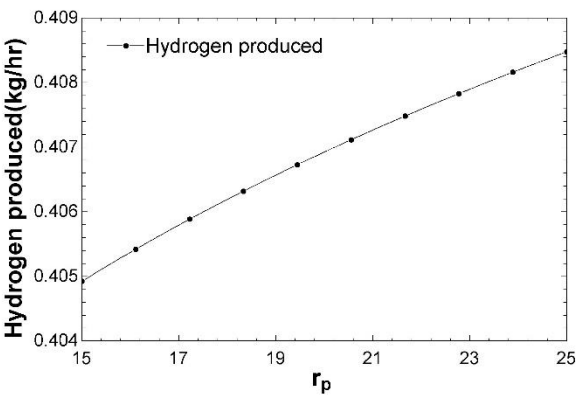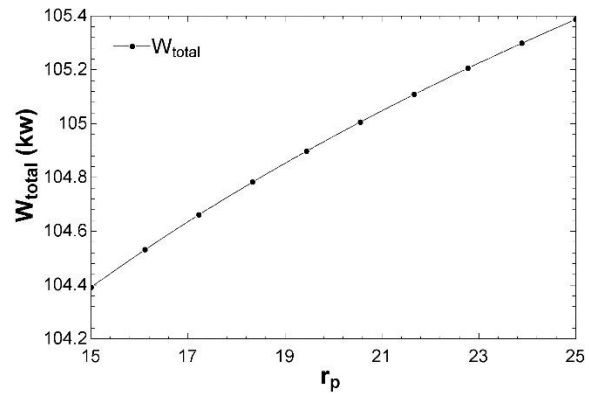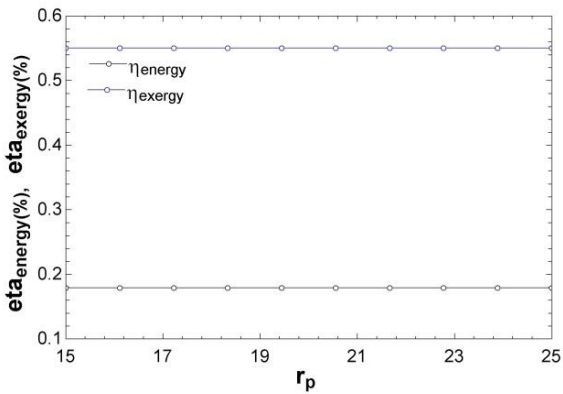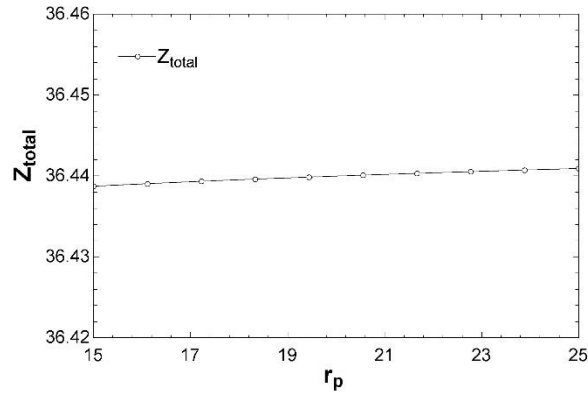
Fig.4. The effect of compressor compression ratio changes on system performance

8.1.4 Effect of compressor isentropic efficiency changes on system performance

Figure 5 examines the impact of varying compressor efficiency on the system's power output, hydrogen production, cost rate, and both energy and exergy efficiency. The results demonstrate that increasing compressor efficiency from 0.7 to 0.9 results in a reduction in both the net power output of the system and the volume of hydrogen produced. This decline in power and hydrogen production is attributed to a chain reaction: decreased compressor efficiency disrupts cycle flow, which in turn slows the cycle process speed, leading to diminished turbine work output at lower operating speeds. Consequently, the reduced electrical power output adversely affects the performance of the electrolyzer, ultimately resulting in decreased hydrogen production. The reduction in exergy occurs because exergy efficiency is directly linked to system output power. Consequently, a decrease in system work results in a corresponding decline in system exergy. Electrolyzers, which are employed in renewable energy systems, produce hydrogen by passing direct current through pure water, thereby splitting it into hydrogen and oxygen through the process of water electrolysis. The exergy of this system quantifies its potential for useful work. A reduction in total work output directly decreases exergy efficiency. Furthermore, this diminished work output allows for the use of less expensive equipment, ultimately reducing the overall operating costs of the system.
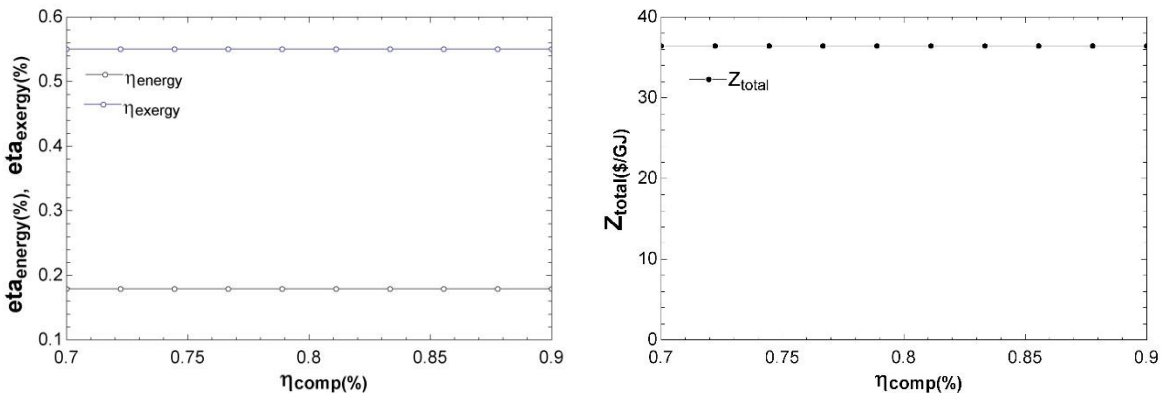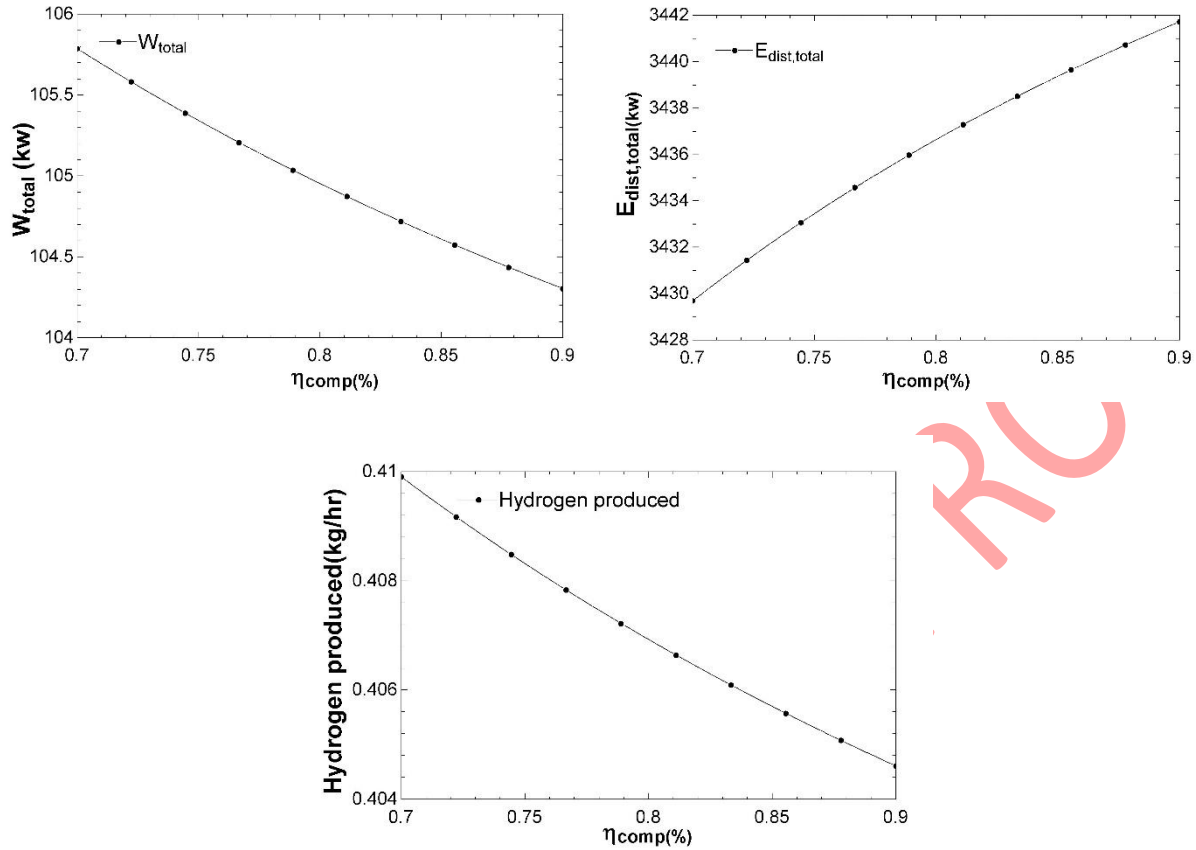
Fig.5. The effect of changes in compressor isentropic efficiency on system performance

8.2 The results of two-objective optimization with genetic algorithm

Optimizing the operating conditions of the proposed system is essential. A genetic algorithm is employed for this purpose, specifically aimed at maximizing exergetic efficiency while minimizing product cost rates. The optimal values obtained are presented in Table 9. Through the application of genetic optimization, the system's performance was improved, achieving optimal energy and exergy efficiencies of 18.4% and 55.5%, respectively. Notably, optimizing the proposed system leads to a reduction in operational costs, resulting in an optimal total cost of $36.46 per GJ. This improvement enhances the economic viability of the system for various industrial applications. Additionally, the TOPSIS decision-making method complements the optimization process by facilitating the identification of the most advantageous position for optimal system performance. The optimal performance of the proposed system, achieved through optimization, is illustrated in Figure 6. This optimal point, marked on the Pareto chart, provides the best combination of low cost and high exergy efficiency. Figures 7 and 8 also present Pareto diagrams that identify the ideal operating conditions for simultaneously reducing electricity and hydrogen production costs while increasing the system's exergy efficiency. The application of

the TOPSIS technique to the optimized results yields a distinct point, highlighted in red, which represents superior system performance when considering all evaluated factors.

Table. 9. Optimization results

parameter	Optimal value
Compressor isentropic efficiency (%)	86
Turbine isentropic efficiency (%)	76
Turbine output pressure (kPa)	48.36
Exergy efficiency (%)	55.5
energy efficiency (%)	18.4
LCOE(cent/kwh)	24.48
LCOH($/kg)	23.94
Total cost ($/GJ)	36.46
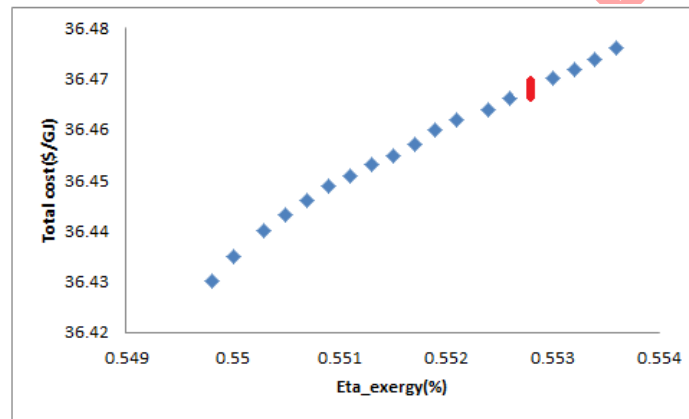
Fig. 6. Pareto diagram considering exergy efficiency and total cost
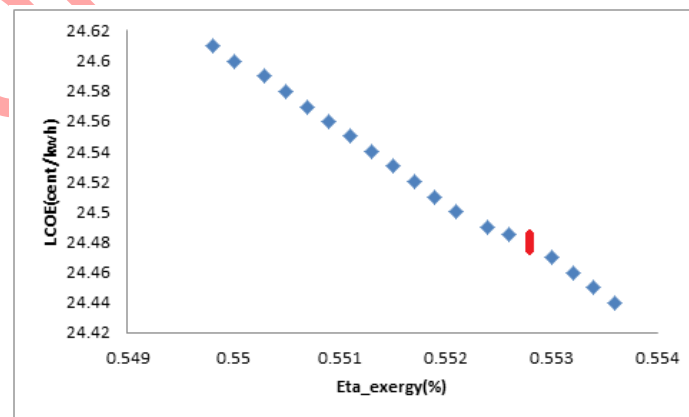
Fig. 7. Pareto diagram considering exergy efficiency and levelized cost of electricity generation
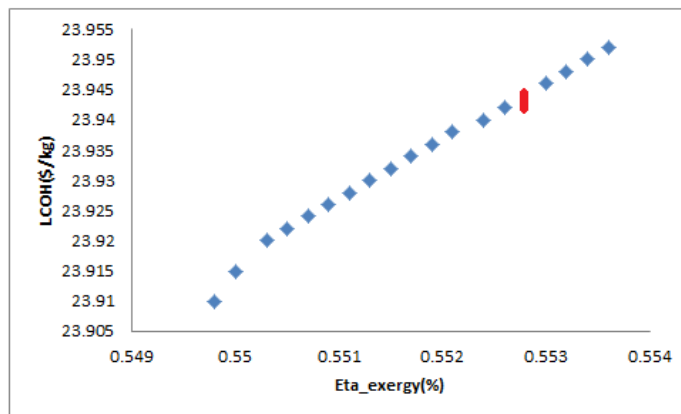
Fig. 8. Pareto diagram considering exergy efficiency and levelized cost of hydrogen production

9.Conclusion

This paper presents a comprehensive thermodynamic development and analysis of a novel multi-generation system that harnesses geothermal energy to co-produce electricity, hydrogen, and cooling. The proposed system comprises a double-flash geothermal unit, two ejector cooling cycles, a proton exchange membrane electrolyzer, an absorption precooling cycle, and a Claude hydrogen liquefaction subsystem. The study highlights the significant yet underexplored potential of binary flash geothermal power plants in advancing the development of these ternary generation systems. This research proposes and evaluates an innovative multi-production system designed for this purpose. The system's feasibility is assessed using thermodynamic principles, and its performance, including that of its subsystems, is thoroughly analyzed under various conditions to identify key findings. Performance evaluation of the system demonstrated an energy efficiency of 21.6% and an exergy efficiency of 54.1%. The output power in the studied system is calculated to be 105 kW, and the total exergy destruction of the system is 3437 kW. The results show that among the system components, the PEM electrolyzer has the highest exergy destruction. The highest share of the cost rate among the system components belongs to the PEM electrolyzer. The economic analysis estimated the total cost of the system to be $37.60 per gigajoule. The investigation examined the effects of variations in key system parameters—including turbine and compressor isentropic efficiency, turbine output pressure, and compressor compression ratio—on overall system performance. The optimization of the proposed system was accomplished using a two-objective genetic algorithm in conjunction with a TOPSIS decision-making process. The genetic algorithm played a crucial role in optimizing the design variable settings, leading to a reduction in overall system costs and an enhancement in the system's exergy efficiency.

Declarations

- ethics approval and consent to participate

  Not applicable

- Consent for publication

  Not applicable

- Availability of data and materials

  The data will be made available on request

- Competing interests

  The authors declare that they have no competing interests

- Funding

  Not applicable

10.References

[1] Chiari L, Zecca A. Constraints of fossil fuels depletion on global warming projections. Energy Policy 2011;39:5026–34.

[2] Hwangbo S, Nam K, Heo S, Yoo C. Hydrogen-based self-sustaining integrated renewable electricity network (HySIREN) using a supply-demand forecasting model and deep-learning algorithms. Energy Convers Manage 2019;185:353–67.

[3] García-Olivares A, Solé J, Osychenko O. Transportation in a 100% renewable energy system. Energy Convers Manage 2018;158:266–85.

[4] G. Axelsson, 7.01 - introduction to volume on geothermal energy. Comprehensive Renewable Energy (Second Edition), Elsevier, Oxford, 2022, pp. 1–2. T. M. Letcher.

[5] T.I. Sigfusson, 7.01 - geothermal energy – introduction. Comprehensive Renewable Energy, Elsevier, Oxford, 2012, pp. 1–2. A. Sayigh.

[6] M.A. Kordlar, et al., Thermo-economic evaluation of a tri-generation system driven by geothermal brine to cover flexible heating and cooling demand, Geothermics 110 (2023) 102678.

[7] S. Zhang, et al., Renewable energy systems for building heating, cooling and electricity production with thermal energy storage, Renew. Sustain. Energy Rev. 165 (2022) 112560.

[8] L. Zhang, et al., Multi-objective particle swarm optimization applied to a solar-geothermal system for electricity and hydrogen production; Utilization of zeotropic mixtures for performance improvement, Process Saf. Environ. Prot. 175 (2023) 814–833.

[9] A. Ebrahimi-Moghadam, et al., Performance investigation of a novel hybrid system for simultaneous production of cooling, heating, and electricity, Sustain. Energy Technol. Assess. 43 (2021) 100931.

[10] Kianfard H, Khalilarya S, Jafarmadar S.Exergy and exergoeconomic evaluation of hydrogen and distilled water production via combination of PEM electrolyzer, RO desalination unit and geothermal driven dual fluid ORC. Energy Conversion and Management, Vol. 177, pp. 339-49, 2018.

[11] Akrami E, Chitsaz A, Nami H, Mahmoudi S. Energetic and exergoeconomic assessment of a multi-generation energy system based on indirect use of geothermal energy. *Energy*, Vol. 124, pp. 625-39, 2017.

[12] Yuksel YE, Ozturk M. Thermodynamic and thermoeconomic analyses of a geothermal energy based integrated system for hydrogen production. *International Journal of Hydrogen Energy*, Vol. 42, pp. 2530-46, 2017.

[13] Ghaebi H, Namin AS, Rostamzadeh H. Performance assessment and optimization of a novel multi-generation system from thermodynamic and thermoeconomic viewpoints. *Energy conversion and management, Vol. 165, pp. 419-39, 2018.*

[14] Yilmaz F, Ozturk M, Selbas R. Modeling and design of the new combined doubleflash and binary geothermal power plant for multigeneration purposes; thermodynamic analysis. Int J Hydrogen Energy 2022;47:19381–96.

[15] Hai T, Radman S, Abed AM, Shawabkeh A, Abbas SZ, Deifalla A, et al. Exergoeconomic and exergo-environmental evaluations and multi-objective optimization of a novel multigeneration plant powered by geothermal energy. Process Saf Environ Protect 2023;172:57–68.

[16] Sangesaraki AG, Gharehghani A, Mehrenjani JR. 4E analysis and machine learning optimization of a geothermal-based system integrated with ejector refrigeration cycle for efficient hydrogen production and liquefaction. Int J Hydrogen Energy 2023.

[17] Coskun A, Bolatturk A, Kanoglu M. Thermodynamic and economic analysis and optimization of power cycles for a medium temperature geothermal resource. Energy Convers Manag 2014;78:39–49.

[18] Abdolalipouradl M, Mohammadkhani F, Khalilarya S, Yari M. Thermodynamic and exergoeconomic analysis of two novel tri-generation cycles for power, hydrogen and freshwater production from geothermal energy. Energy Convers Manag 2020; 226.

[19] Rostamzadeh H, Ghaebi H, Vosoughi S, Jannatkhah J. Thermodynamic and thermoeconomic analysis and optimization of a novel dual-loop power/ refrigeration cycle. Appl Therm Eng 2018;138:1–17.

[20] Pan D, Gholami Farkoush S. Comprehensive analysis and multi-objective optimization of power and cooling production system based on a flash-binary geothermal system. Appl Therm Eng 2023:120398.

[21] Zhang M, Timoshin A, Al-Ammar EA, Sillanpaa M, Zhang G. Power, cooling, freshwater, and hydrogen production system from a new integrated system working with the zeotropic mixture, using a flash-binary geothermal system. Energy 2023;263.

[22] Yilmaz F, Ozturk M. Modeling and parametric analysis of a new combined geothermal plant with hydrogen generation and compression for multigeneration. Int J Hydrogen Energy 2023.

[23] Heidarnejad, P., Genceli, H., Asker, M., Khanmohammadi, S., 2020, A comprehensive approach for optimizing a biomass assisted geothermal power plant with freshwater production: Techno-economic and environmental evaluation, Energy Conversion and Management 226, 113514.

[24] Kahraman, M., BahadırOlcay, A., Sorguven, E., 2019, Thermodynamic and thermoeconomic analysis of a 21MW binary type aircooledgeothermal power plant and determination of the effect of ambienttemperature variation on the plant performance, Energy Conversion and Management 192, 308–320.

[25] Design and analysis of a novel multi-generation plant utilising geothermal energy Fatih Yilmaz, Murat Ozturk, and Resat Sebas International Journal of Exergy 2024 45:3-4, 296-310.

[26] Yılmaz, Fatih & Ozturk, Murat & Selbaş, Reşat. (2023). Thermodynamic and exergoenvironmental assessment of an innovative geothermal energy assisted multigeneration plant combined with recompression supercritical CO2 Brayton cycle for the production of cleaner products. International Journal of Hydrogen Energy. 75. 10.1016/j.ijhydene.2023.12.048.

[27] Dan, Ma & He, Ang & Ren, Qiliang & Li, Wenbo & Huang, Kang & Wang, Xiangda & Feng, Boxuan & Sardari, Farshid. (2024). Multi-aspect evaluation of a novel double-flash geothermally-powered integrated multigeneration system for generating power, cooling, and liquefied Hydrogen. Energy. 289. 129900. 10.1016/j.energy.2024.129900.

[28] H. Rostamzadeh, A. S. Namin, H. Ghaebi, and M. Amidpour, "Performance assessment and optimization of a humidification dehumidification (HDH) system driven by absorption-compression heat pump cycle," *Desalination,* vol. 447, pp. 84-101, 2018.

[29] A. Nemati, R. Mohseni, and M. Yari, "A comprehensive comparison between CO2 and Ethane as a refrigerant in a two-stage ejector-expansion transcritical refrigeration cycle integrated with an organic Rankine cycle (ORC)," *The Journal of Supercritical Fluids, vol. 133, pp. 494-502, 2018.*

[30] H. Ghaebi, T. Parikhani, H. Rostamzadeh, and B. Farhang, "Thermodynamic and thermoeconomic analysis and optimization of a novel combined cooling and power (CCP) cycle by integrating of ejector refrigeration and Kalina cycles," *Energy,* vol. 139, pp. 262-276, 2017.

[31] Boyaghchi F. A., M. Chavoshi, and V. Sabeti, "Multi-generation system incorporated with PEM electrolyzer and dual ORC based on biomass gasification waste heat recovery: Exergetic, economic and environmental impact optimizations," *Energy*, vol. 145, pp. 38–51, 2018.

[32] M. Sharaf, M.S. Yousef, A.S. Huzayyin, Year-round energy and exergy performance investigation of a photovoltaic panel coupled with metal foam/phase change material composite, Renew. Energy (2022).

[33] M. Noaman, G. Saade, T. Morosuk, G. Tsatsaronis, Exergoeconomic analysis applied to supercritical CO2 power systems, Energy 183 (2019) 756–765.

[34] Nemati A, Sadeghi M, Yari M. Exergoeconomic analysis and multi-objective optimization of a marine engine waste heat driven RO desalination system integrated with an organic Rankine cycle using zeotropic working fluid. Desalination 2017;422:113–23.

[35] O.L. Gulder, "Flame temperature estimation of conventional and future jet fuels", Journal of Engineering for Gas Turbine and Power, 1986; 108(2), 376-380.

[36] H. Sayyadi, "Multi-objective approach in thermoenvironomic optimization of a benchmark cogeneration system", Applied Energy, 2009; 86(6), 867-879.

[37] Lingbao Wang, Xianbiao Bu, Hanzhi Wang, Zhitong Ma, Weibin Ma, Huashan Li, (2018). Thermoeconomic evaluation and optimization of LiBr-H2O double absorption heat transformer driven by flat plate collector, *Energy Conversion and Management* 162. 66–76.

[38] Razmi AR, Janbaz M. Exergoeconomic assessment with reliability consideration of a green cogeneration system based on compressed air energy storage (CAES). Energy Convers Manag 2019:112320.

[39] H. Kianfard, S. Khalilarya, S. Jafarmadar, Exergy and exergoeconomic evaluation of hydrogen and distilled water production via combination of PEM electrolyzer, RO desalination unit and geothermal driven dual fluid ORC, Energy Convers. Manag. 177 (2018) 339–349, vol.

[40] A. Arora, S.C. Kaushik. Theoretical analysis of LiBr/H2O absorption refrigeration systems. International Journal of Energy Research vol. 9, pp. 1321–1340, 2009.